JOINT ENCODING LBP FEATURES FROM INFRARED AND VISIBLE-LIGHT CLOUD IMAGE OBSERVATIONS FOR GROUND-BASED CLOUD CLASSIFICATION

Yu Wang, Chunheng Wang, Cunzhao Shi, and Baihua Xiao

State Key Laboratory of Management and Control for Complex Systems, Institute of Automation, Chinese Academy of Sciences, Beijing 100190, P. R. China
University of Chinese Academy of Sciences, Beijing 100190, P. R. China
School of Software, Shanxi University, Taiyuan 030006, P. R. China

ABSTRACT

Cloud type classification based on ground-based cloud image observations is an important task in atmospheric research. Currently, two kinds of cloud image observations with infrared and visible light images are widely used for cloud classification. However, they are only independently analyzed and simply compared in the current study. The useful information from these two kinds of images is not fully utilized and integrated. The classification performance could be improved if taking full advantage of the complementary information of these two observations. Thus, first, a database containing these two kinds of cloud images with same temporal resolution is released in this study. Then, a two-observation joint encoding strategy of LBP (local binary pattern) features is proposed to implement cloud classification by encoding the joint distribution of LBP patterns in different observations, which captures the correlation between two observations. Experimental results based on this database show the significant superiority of the proposed method compared to the results based on the single observation.

***Index Terms*—** Local binary patterns, joint distribution, cloud classification, visible light, infrared cloud images

1. INTRODUCTION

In recent years, ground-based image observations of clouds have become increasingly popular. Because these images are available at low cost and high resolution, and they offer accurate local and short-term cloud information ([1, 2]). Cloud height, cloud cover, and cloud type are three important factors for ground-based cloud observation. In this study, we focus on the research of cloud type. The timely and accurate cloud type classification has a great significance on the weather prediction and the understanding of climatic conditions([3, 4, 5]).

Currently, ground-based cloud image observations generally include two ways of infrared and visible light. Visible light images provide the most direct and accurate observation for clouds, however, they are easily affected by visibility and aerosol. Infrared images gain the cloud information by using the 8-14 μm band infrared radiation, and they can achieve the 24 hours' continuous observation. These two kinds of cloud image observations attain different useful information of clouds. However, they are only independently analyzed and simply compared in the current study. The useful information is not fully utilized and integrated. Thus, the classification performance could be improved if taking full advantage of the complementary information of these two observations.

Extracting effective features is a fundamental issue in image analysis. In particular, a local texture descriptor, called local binary pattern (LBP)([6]), has gained much attention due to its low computational complexity, gray-scale and rotation invariance, robustness, and excellent performance in many applications ([7, 8, 9, 10]). Thus, in this study, LBP features are introduced to the classification of cloud images.

To integrate cloud texture information in two kinds of different observations, a concatenated strategy similar to multi-scale strategy is a natural choice ([11]). However, this simply concatenated strategy ignores the correlation information between different observations. In fact, texture patterns in different image observations clearly have a strong correlation, because visible light and infrared cloud images are taken at the same time and place. Ignoring such correlation may lead to the loss of the useful discriminative information of cloud type classification. Thus, in this study, we propose a two-observation joint encoding strategy of LBP (TOJ-LBP) feature to encode the joint distribution of LBP patterns in different image observations.

2. TWO-OBSERVATION JOINT ENCODING OF LOCAL BINARY PATTERNS

2.1. A simple review of LBP operator

LBP is an effective gray-scale and rotation invariant texture operator that depicts local structures of natural texture im-

This work was supported in part by the National Natural Science Foundation of China (NSFC) under Grant Nos. 61531019, 61503228, 61601462, and 71621002. Chunheng Wang is the corresponding author.

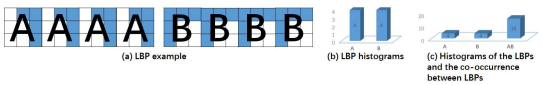

Fig. 1. Difference of LBP histogram and integrated histogram of LBPs and co-occurrence LBPs.

ages. The LBP patterns can be computed by comparing its pixel value with the values of its neighbors:

$$LBP_{P,R} = \sum_{p=0}^{P-1} s(g_p - g_c)2^p,\ s(x) = \begin{cases} 1 & x \geq 0 \\ 0 & x < 0, \end{cases} \quad (1)$$

where g_c and $g_p,\ p = 0, \ldots, P-1$ are the gray values of center pixel and neighboring pixels on a circle of radius $R(R > 0)$ from a circularly neighbor set.

To achieve robustness to image rotation, a uniform gray scale and rotation invariant texture descriptor is introduced by defining a uniformity measure U

$$LBP^{riu2}_{P,R} = \begin{cases} \sum_{p=0}^{P-1} s(g_p - g_c) & \text{if } U(LBP_{P,R}) \leq 2 \\ P+1 & \text{otherwise} \end{cases} \quad (2)$$

where

$$\begin{aligned} U(LBP_{P,R}) &= |s(g_{P-1} - g_c) - s(g_0 - g_c)| \\ &+ \sum_{p=1}^{P-1} |s(g_p - g_c) - s(g_{p-1} - gc)|. \end{aligned}$$

For example, for the number of neighbors P=8, LBP has 36 rotation invariant patterns, in which there are 9 uniform patterns and 27 non-uniform patterns.

2.2. Two-observation joint encoding of LBP patterns

To capture the texture information in different observations, a two-observation concatenation strategy is a natural choice. First, the LBP histograms are extracted individually from each observation, and then the histograms for two observations are concatenated into the final representation.

Unfortunately, however, the correlations among the LBP patterns with different observations are ignored during the LBP histogram generation process. For example, the LBP patterns in two observations of visible light and infrared cloud images are composed of four LBP A and four LBP B patterns, respectively, as shown in Fig. 1 (a). Then, the concatenated LBP histograms are generated by a direct concatenated operation as shown in Fig.1(b). In contrast to the histograms of the co-occurrence LBP patterns extracted from two observations shown in Fig.1(c), the original concatenated LBP histograms obviously lose some important information. This also suggests that the expression ability of the original LBP is insufficient, and there is still a room for further improvement to the performance of LBP-based features.

To characterize stronger image texture features, it is necessary to jointly encode the joint distribution of LBP patterns in different observations. Here, we propose a two-observation joint encoding strategy of local binary pattern (TOJ-LBP) features. Denote TOJ-LBP with observations s_1 and s_2 as $TOJ_{LBP}(s_1, s_2)$, then it can be defined as follows:

$$\begin{aligned} TOJ_{LBP}(s_1, s_2) &= \Big[LBP^{(s_1)}_{P,R}, LBP^{(s_2)}_{P,R}, \\ &\quad [LBP^{(s_1)}_{P,R}, LBP^{(s_2)}_{P,R}]_{co}\Big] \end{aligned} \quad (3)$$

where s_1 and s_2 refer to the ground-based visible light and infrared observations, respectively. $LBP_{P,R}(\cdot)$ refer to the rotation invariant uniform LBP patterns. $[,]_{co}$ refer to the co-occurrence LBP patterns. For example, as indicated before, $LBP^{riu2}_{8,1}$ and $LBP^{riu2}_{16,2}$ have 10 and 18 patterns, respectively. Thus, $[LBP^{(s_1)}_{P,R}, LBP^{(s_2)}_{P,R}]_{co}$ would include $10 \times 10 = 100$ and $18 \times 18 = 324$ co-occurrence patterns for $P = 8$ and $P = 16$, respectively. And the TOJ-LBP would contain 120 and 360 patterns.

The cloud images can be represented by the corresponding LBP histogram feature vector:

$$f(s_1, s_2) = \left[h_{LBP^{(s_1)}_{P,R}}, h_{LBP^{(s_2)}_{P,R}}, h_{[LBP^{(s_1)}_{P,R}, LBP^{(s_2)}_{P,R}]_{co}}\right] \quad (4)$$

where $h_{LBP^{(s_1)}_{P,R}}$ denotes the histogram for visible light observation, and its element

$$h_{LBP^{(s_1)}_{P,R}}(i) = \sum_{x,y \in I} B(LBP_{P,R}(x, y) = i),\ i \in [1, L], \quad (5)$$

Boolean indicator

$$B(v) = \begin{cases} 1 & when\ v\ is\ true \\ 0 & otherwise, \end{cases} \quad (6)$$

L is the size of rotation invariant uniform LBP patterns. The histograms for infrared and joint observations have similar expression with Eq. (5).

2.3. Dimension reduction

The co-occurrence texture information encoded by TOJ-LBP forms high dimensional feature vectors compared to traditional uniform LBP features. Correspondingly, some redundant or noised information is inevitably introduced in this process. Therefore, we perform dimension reduction on the extracted co-occurrence LBP feature vector before performing classification. Principal component analysis (PCA) is a commonly used way to reduce the dimensions of the feature vectors. Suppose that the matrix corresponding to the original data set X has D_1 dimensions, the PCA will select the first D_2 eigenvectors corresponding to the first largest D_2 eigenvalues of the matrix $X^T X$. The criterion to select D_2 is usually based on the following equation:

$$\frac{\sum_{k=1}^{D_2} |\lambda_k|}{\sum_{k=1}^{D_1} |\lambda_k|} > \theta \quad (7)$$

where λ_k denotes the kth eigenvalue of the matrix $X^T X$, and θ is a threshold value such as 95%.

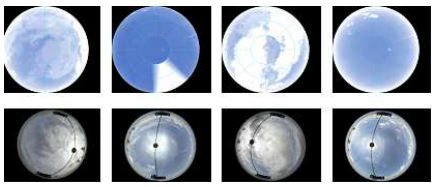

Fig. 2. Some infrared and visible light cloud image samples.

3. EXPERIMENTAL EVALUATION

3.1. Database and experimental setup

In this domain, we do not find public benchmarking database containing both visible light and infrared cloud image observations with same temporal resolution. In view of this problem, we create a database with 591 $\times$ 2 cloud image samples.

The images are stored in a color JPEG format with the resolutions of 2272 $\times$ 1704 and 738 $\times$ 650 pixels, respectively. As such, these images are rectangular in shape, but the whole sky mapped is circular. All images are captured in Yangjiang, Guangdong province of China. In the course of this observation, four different sky conditions of stratiform, undulatus, and cirriform clouds, and mixed sky conditions are covered. The sample sizes for each cloud type are 231, 23, 272, and 65, respectively. Some representative images from each category are shown in Fig. 2.

In this study, the kernel support vector machine (KSVM) and multi-level perceptron (MLP) are chosen([4]). For effectively evaluating the performance of the extracted features and algorithms, the widely used Leave-One-Out Cross-validation (LOOCV) are applied ([3]). Specifically, for a training sample set T with the size of n, if one single element t is removed, the algorithm is trained with the remaining data set $T-t$. This process is repeated n times. The average number of correctly classified elements can be expressed

$$LOOCV = \frac{|\{t \in T | t\ is\ classified\ correctly\}|}{n} \qquad (8)$$

3.2. Experimental Results

With the released database, we provide the total and the respective class classification results based on the LOOCV for the rotation invariant uniform LBP patterns on the single and joint observations. In view of the computation cost and the representation of circular neighbor in LBP patterns, we select $(P = 8, R = 1)$, $(P = 16, R = 2)$ and $(P = 24, R = 3)$ three combinations.

Table 1. Classification performance on KSVM Classifier %

Method	Class				
	1	2	3	4	Average
$LBP^{riu2}_{8,1}$(infrared)	57.6	47.8	80.1	83.1	70.4
$LBP^{riu2}_{8,1}$(visible light)	57.6	0.0	71.3	60.0	61.9
$LBP^{riu2}_{8,1}$(infrared+visible light)	56.3	30.4	82.0	78.5	69.5
$LBP^{riu2}_{8,1}$(infrared+visible light+co-occurrence)	55.8	39.1	83.1	78.5	70.4
$LBP^{riu2}_{8,1}$(infrared+visible light+co-occurrence+pca)	64.9	73.9	82.3	81.5	**75.1**
$LBP^{riu2}_{16,2}$(infrared)	61.0	65.2	82.3	78.5	72.9
$LBP^{riu2}_{16,2}$(visible light)	53.2	0.0	74.6	64.6	62.3
$LBP^{riu2}_{16,2}$(infrared+visible light)	57.1	52.2	84.2	78.5	71.7
$LBP^{riu2}_{16,2}$(infrared+visible light+co-occurrence)	58.0	65.2	83.0	78.5	72.1
$LBP^{riu2}_{16,2}$(infrared+visible light+co-occurrence+pca)	71.4	86.9	84.2	86.2	**79.5**
$LBP^{riu2}_{24,3}$(infrared)	71.4	65.2	83.1	76.9	77.2
$LBP^{riu2}_{24,3}$(visible light)	61.0	0.0	72.4	60.0	63.8
$LBP^{riu2}_{24,3}$(infrared+visible light)	63.6	73.9	83.8	80.0	75.1
$LBP^{riu2}_{24,3}$(infrared+visible light+co-occurrence)	63.8	69.6	84.2	77.3	75.3
$LBP^{riu2}_{24,3}$(infrared+visible light+co-occurrence+pca)	71.9	86.9	86.8	86.0	**81.0**

Table 2. Classification performance on MLP Classifier %

Method	Class				
	1	2	3	4	Average
$LBP^{riu2}_{8,1}$(infrared)	61.0	78.3	82.3	89.2	74.6
$LBP^{riu2}_{8,1}$(visible light)	58.0	17.4	77.9	56.9	65.5
$LBP^{riu2}_{8,1}$(infrared+visible light)	63.2	82.6	79.0	76.9	72.8
$LBP^{riu2}_{8,1}$(infrared+visible light+co-occurrence)	65.4	91.3	78.7	81.5	74.3
$LBP^{riu2}_{8,1}$(infrared+visible light+co-occurrence+pca)	69.3	91.3	81.6	81.5	**77.8**
$LBP^{riu2}_{16,2}$(infrared)	69.3	82.6	80.9	84.6	76.8
$LBP^{riu2}_{16,2}$(visible light)	52.2	30.4	72.8	73.8	63.3
$LBP^{riu2}_{16,2}$(infrared+visible light)	71.0	87.0	80.9	83.1	77.5
$LBP^{riu2}_{16,2}$(infrared+visible light+co-occurrence)	71.1	95.7	80.9	80.5	77.5
$LBP^{riu2}_{16,2}$(infrared+visible light+co-occurrence+pca)	72.1	95.5	86.5	89.0	**81.5**
$LBP^{riu2}_{24,3}$(infrared)	73.6	73.9	83.1	81.5	78.8
$LBP^{riu2}_{24,3}$(visible light)	56.7	17.4	75.4	63.1	64.5
$LBP^{riu2}_{24,3}$(infrared+visible light)	73.6	87.0	82.6	80.0	79.2
$LBP^{riu2}_{24,3}$(infrared+visible light+co-occurrence)	73.7	94.6	83.0	84.7	80.0
$LBP^{riu2}_{24,3}$(infrared+visible light+co-occurrence+pca)	77.4	92.3	88.8	89.9	**84.6**

3.2.1. Results on KSVM classifier

Table 1 shows the classification results of five techniques for three cases of $(P = 8, R = 1)$, $(P = 16, R = 2)$ and $(P = 24, R = 3)$ on KSVM classifier. First, we can see that if extracting LBP features only from visible light cloud images, the traditional $LBP^{riu2}_{8,1}$ method exhibits the worst classification performance with only 61.9%. For the infrared cloud images, the total classification performance of $LBP^{riu2}_{8,1}$ elevates about 8.5 points from 61.9% to 70.4%. By directly concatenating the LBP features from two observations of infrared and visible light cloud images into a final feature vector, the $LBP^{riu2}_{8,1}$ shows a slightly lower performance than that of the $LBP^{riu2}_{8,1}$(infrared). It is clear that this feature integration does not bring the improvement of classification accuracy. In fact, this is because this simple integration could not add the co-occurrence information into the final feature vector. Thus, a two-observation joint encoding strategy is proposed by considering the joint distribution of LBP patterns in different observations in this study.

However, unfortunately, this direct joint encoding does not also receive the superior classification performance. It only achieves similar classification accuracy (70.4%) with the $LBP^{riu2}_{8,1}$(infrared). This is because although this operation captures the co-occurrence texture information from two ob-

servations, it also introduces the dimensional pressure compared to the traditional uniform LBP features. Correspondingly, some redundant or noised information is inevitably introduced in this process. Therefore, we should perform dimension reduction on the extracted co-occurrence LBP feature vector before performing classification. Experimental results validate this point. The classification accuracy of the proposed method increases about five percentage points from 70.4% to 75.1% after the dimension of the TOJ-LBP features is reduced from 100 to 18.

When the (P, R) varies from $(8, 1)$ to $(16, 2)$, whether for infrared and visible light observations, or for their integration, the total classification accuracies all elevate about two percentage points. The proposed method with PCA further elevates 4.4% corresponding to the case of $(P, R) = (8, 1)$. The best classification performance of our method rises by 7.5%, 18.3%, 8.9%, and 8.4% relative to the performances of other methods on three combinations of (P, R), respectively.

Table 1 also presents the results of each class based on the LOOCV. For types 3 and 4, our method achieves 80% accuracy. For type 2, in all three cases, the traditional LBP exhibits the worst performance for visible light cloud images that all samples are misclassified. However, by integrating the LBP patterns from infrared images and the co-occurrence patterns from infrared and visible light images, our method reaches to 86.9% accuracy. In all four cloud types, the classification results of type 1 are the worst. The classification accuracies of the proposed method are only 64.9%, 71.4% and 71.9% for three cases, respectively. By observing the confusion matrix, we find that type 1 is easily misclassified as types 2 and 3.

3.2.2. Results on MLP classifier

For the MLP classifier, all methods show better performance than that on the SVM classifier. For example, in contrast to the classification performance on SVM classifier for single infrared observation, the total and the respective class classification accuracies lift 4.2%, 3.4%, 30.5%, 2.2%, and 6.1%, respectively. In particular, as shown in Table 2, for type 2, the accuracies of LBP^{riu2}(visible light) are no longer zero, and they varies from zero to 17.4% and 30.4%.

Furthermore, the performances of the proposed method are superior to other methods in three cases of $(8, 1)$, $(16, 2)$, and $(24, 3)$. They are 77.8%, 81.5%, and 84.6%, respectively. Similar to the SVM classifier, in all four cloud types, the worst classification results are still type 1. The maximum improvement arises in type 2. For types 2, 3, and 4, all methods with the co-occurrence patterns show a performance of more than 80% (the type 3 is 78.7% in the case of $(8, 1)$).

In a word, the proposed method achieves the best performance with accuracy 84.6% in the case of $(P, R) = (24, 3)$ on MLP classifier. In future study, we will extend the proposed two-observation joint encoding strategy to other LBP type methods such as local texture patterns (LTP).

4. REFERENCES

[1] S. Dev, "Wahrsis: A low-cost high-resolution whole sky imager with near-infrared capabilities," in *SPIE Defense + Security*, 2014, p. 90711L.

[2] S. Dev, F. M. Savoy, Y. H. Lee, and S. Winkler, "Design of low-cost, compact and weather-proof whole sky imagers for high-dynamic-range captures," in *IEEE Geoscience and Remote Sensing Symposium*. IEEE, 2015, pp. 5359–5362.

[3] A. Heinle, A. Macke, and A. Srivastav, "Automatic cloud classification of whole sky images," *Atmospheric Measurement Techniques*, vol. 3, no. 3, pp. 557–567, 2010.

[4] A. Taravat, F. D. Frate, C. Cornaro, and S. Vergari, "Neural networks and support vector machine algorithms for automatic cloud classification of whole-sky ground-based images," *IEEE Geoscience and Remote Sensing Letters*, vol. 12, no. 3, pp. 666–670, 2015.

[5] S. Dev, B. Wen, Y. H. Lee, and S. Winkler, "Machine learning techniques and applications for ground-based image analysis," *IEEE Geoscience and Remote Sensing Magazine*, vol. 4, no. 2, pp. 79–93, 2016.

[6] T. Ojala, M. Pietikainen, and T Maenpaa, "Multiresolution gray-scale and rotation invariant texture classification with local binary patterns," *IEEE Transactions on Pattern Analysis and Machine Intelligence*, vol. 24, no. 7, pp. 971–987, 2002.

[7] S. Liao, M. W. Law, and A. C. Chung, "Dominant local binary patterns for texture classification.," *IEEE Transactions on Image Processing*, vol. 18, no. 5, pp. 1107–1118, 2009.

[8] X. Tan and B. Triggs, "Enhanced local texture feature sets for face recognition under difficult lighting conditions," *IEEE transactions on image processing*, vol. 19, no. 6, pp. 1635–1650, 2010.

[9] K. C. Fan and T. Y. Hung, "A novel local pattern descriptor–local vector pattern in high-order derivative space for face recognition.," *IEEE Transactions on Image Processing*, vol. 23, no. 7, pp. 2877–2891, 2014.

[10] X. Qi, R. Xiao, C. Li, and Y. Qiao, "Pairwise rotation invariant co-occurrence local binary pattern," *IEEE Transactions on Pattern Analysis and Machine Intelligence*, vol. 36, no. 11, pp. 2199–2213, 2014.

[11] J. T. Kwak, S. Xu, and B. J. Wood, "Efficient data mining for local binary pattern in texture image analysis.," *Expert Systems with Applications*, vol. 42, no. 9, pp. 4529–4539, 2015.